Power System Protection and Control
ISSN:1674-3415

# KINEMATIC OPTIMISATION OF SOFT ROBOTIC MANIPULATORS FOR MEDICAL INTERVENTION

**Sai Akshara Vemuri**

George W. Woodruff School of Mechanical Engineering
Georgia Institute of Technology, Atlanta, Georgia, USA

**Received**: 07/05/2026 **Revised**: 10/06/2026 **Accepted**: 02/07/2026

***ABSTRACT*:**

Soft robotic manipulators are increasingly investigated for minimally invasive medical intervention because their intrinsic compliance allows safe interaction with delicate anatomical structures while their continuum architecture enables navigation through tortuous natural or surgically created pathways. However, the same compliance that confers safety also introduces kinematic redundancy, nonlinear actuation-to-shape mappings, and configuration-dependent stiffness that complicate motion planning and control. This paper presents a unified kinematic optimisation framework for tendon-driven and hybrid-stiffness soft manipulators intended for confined-space medical procedures such as laparoscopy, endoluminal navigation, and transoral surgery. Building on piecewise constant-curvature (PCC) and Cosserat-rod continuum formulations, we develop a multi-objective optimisation formulation that simultaneously maximises reachable dexterous workspace, minimises tip positioning error under external tissue-contact loading, and regulates task-space stiffness through auxiliary backbone insertion. The Jacobian-based manipulability and compliance-ellipsoid formulations are used to construct differentiable cost terms suitable for gradient-based and evolutionary optimisation. A representative case study—navigation of a dual-segment tendon-driven manipulator toward a simulated pancreatic target through a constrained laparoscopic port—is used to illustrate the framework. Results indicate that joint kinematic-and-stiffness optimisation improves the trade-off between reachability and positional accuracy relative to single-objective curvature optimisation, while remaining computationally tractable for pre-operative planning. The paper concludes with a discussion of open challenges, including real-time re-optimisation under tissue deformation and the incorporation of contact-rich Cosserat models into the optimisation loop.

***Keywords***: *Soft Robotics, Continuum Manipulators, Kinematic Optimisation, Cosserat Rod Theory, Minimally Invasive Surgery, Compliance Ellipsoid, Tendon-Driven Robots*

## INTRODUCTION

Robot-assisted minimally invasive surgery (MIS) has matured over three decades from early laparoscopic camera holders to fully articulated, teleoperated rigid-link systems capable of sub-millimetre precision. Despite these advances, rigid-link robotic instruments remain fundamentally constrained by their kinematic architecture: each additional degree of freedom (DoF) requires a discrete joint, actuator, and transmission, all of which must be miniaturised to fit through small-diameter ports or natural orifices. This constraint becomes acute when a procedure requires the instrument to traverse curved anatomical channels, operate in confined cavities, or make gentle, compliant contact with friable tissue such as pancreatic parenchyma, neural bundles, or vascular walls.

Soft and continuum robotic manipulators address this limitation by distributing bending compliance along an elastomeric or superelastic backbone rather than concentrating it at discrete joints. Because deformation is continuous, a soft manipulator can, in principle, assume an infinite family of smooth shapes using a comparatively small number of actuators (tendons, pneumatic chambers, or concentric pre-curved tubes). This property is highly attractive for medical applications: the manipulator can conform to curved lumens, distribute contact forces over a larger surface area, and reduce the risk of tissue perforation relative to a rigid instrument of equivalent reach.

The price of this compliance is a substantially more complex relationship between actuation input and manipulator shape. Unlike rigid serial manipulators, whose forward kinematics is a closed-form composition of homogeneous transformations parameterised by a finite joint vector, a soft manipulator's configuration is, strictly speaking, an infinite-dimensional object—a continuous curve in $SE(3)$governed by the equilibrium of internal elastic forces, external loads (gravity, tissue contact, insufflation pressure), and actuator forces. Practical modelling therefore relies on reduced-order approximations: piecewise constant-curvature (PCC) kinematics for fast, closed-form estimates, and Cosserat-rod mechanics for higher-fidelity prediction of shape under external loading. Both formulations expose a *kinematic optimisation problem*: given a desired task (reach a target, avoid an obstacle, deliver a fibre-optic tip at a prescribed orientation, or grasp tissue with bounded contact force), what actuation trajectory and, where available, auxiliary stiffness-modulation input best satisfies the task while respecting the manipulator's physical constraints?

This paper develops a kinematic optimisation framework tailored to medical intervention scenarios. Three features distinguish medical applications from generic continuum-robot motion planning and motivate the specific formulation adopted here. First, the *workspace* that must be reached is typically small and irregularly bounded by rigid anatomical structures (bone, trocar geometry, adjacent organs), so optimisation must explicitly balance reachability against collision avoidance. Second, the *manipulator must exert or withstand external loads*—for example, gentle retraction of tissue, or the reaction force of a diffusing fibre pressed against a target for photodynamic or thermal therapy—so the optimisation objective must include a task-space stiffness or compliance term, not merely a positional error term. Third, many practical soft-manipulator designs used clinically or pre-clinically incorporate a secondary stiffness-modulation mechanism, such as a slidable superelastic backbone or a controllable phase-change layer, which introduces an additional decision variable that trades reachable workspace against resistance to deflection under load. The framework below treats this stiffness-modulation depth as a first-class optimisation variable alongside the tendon actuation vector.

The remainder of the paper is organised as follows. Section 2 reviews prior work on continuum-robot kinematics and optimisation-based motion planning for medical soft robots. Section 3 develops the kinematic models used in this study, covering both PCC and Cosserat-rod formulations. Section 4 formulates the multi-objective kinematic optimisation problem, including the manipulability and compliance-ellipsoid cost terms. Section 5 describes the numerical optimisation procedure. Section 6 presents an illustrative case study of laparoscopic targeting. Section 7 discusses results and limitations, and Section 8 concludes.

## RELATED WORK

### 2.1 Continuum Robot Kinematics

Early continuum-robot kinematics relied on the constant-curvature assumption, under which each manipulator section is modelled as a circular arc of constant curvature $\kappa$, and the full-shape forward kinematics reduces to a composition of a small number of homogeneous transformations parameterised by curvature, bending-plane angle, and arc length. This approach yields closed-form Jacobians and remains widely used for real-time control because of its computational efficiency, although it neglects the effect of external loads, gravity sag, and material nonlinearity, all of which are significant when a manipulator contacts tissue.

To capture load-dependent deformation, several groups adopted the Cosserat-rod formulation, which models the manipulator as a one-dimensional elastic rod subject to distributed and point forces and moments, coupled with tendon or fluidic actuation models. This approach yields a two-point boundary-value problem typically solved via a shooting method, and has been validated for tendon-driven continuum robots, concentric-tube robots, and, more recently, hybrid designs that combine a compliant elastomeric body with a slidable stiff backbone to achieve on-demand stiffness modulation without permanently altering the intrinsic compliance of the body. Finite-element approaches offer a third alternative, trading closed-form efficiency for the ability to model fully three-dimensional, potentially anisotropic elastomeric bodies, at higher computational cost.

### 2.2 Stiffness Modulation Mechanisms

Because pure elastomeric continuum robots are inherently compliant, several stiffness-modulation strategies have been proposed to allow a soft manipulator to bear or transmit load once positioned: thermally activated shape-memory materials and low-melting-point alloys; magneto- and electro-rheological fluids; granular- or layer-jamming mechanisms; antagonistic actuation; and slidable rigid or superelastic backbones inspired by concentric-tube robot design. Backbone-insertion approaches are attractive for medical use because they achieve fast, low-voltage, electromechanically actuated stiffness change without the bulk of jamming pumps or the safety concerns of high electric fields, and because stiffness can be varied continuously during manipulation rather than only after a target pose is reached.


DOI: 10.46121/pspc.54.3.16

Power System Protection and Control
ISSN:1674-3415

### 2.3 Optimisation-Based Planning for Medical Continuum Robots

Motion-planning research for continuum and concentric-tube robots has explored trajectory optimisation for path following, obstacle-aware inverse kinematics, and design optimisation of manipulator geometry (tube curvature, segment length, number of segments) for a specified anatomical workspace. Comparatively less attention has been given to *joint* optimisation of kinematic actuation and stiffness-modulation depth, despite the fact that many recent hybrid-stiffness designs expose insertion depth as an independently controllable variable. This paper addresses that gap by formulating stiffness-modulation depth as an optimisation variable alongside tendon tension, and by explicitly incorporating a compliance-ellipsoid penalty that reflects the manipulator's resistance to deflection under anticipated tissue-contact loads.

## KINEMATIC MODELLING OF SOFT MANIPULATORS

### 3.1 Piecewise Constant-Curvature Kinematics

For a manipulator composed of $N$sections, each of length $\ell_i$, the shape of section $i$is parameterised by curvature $\kappa_i$and bending-plane angle $\phi_i$. The homogeneous transformation from the base of section $i$to its tip is

$$T_i(\kappa_i, \phi_i, \ell_i) = \begin{bmatrix} R_i(\kappa_i, \phi_i) & p_i(\kappa_i, \phi_i, \ell_i) \\ 0 & 1 \end{bmatrix} \qquad (1)$$

where

$$p_i = \frac{1}{\kappa_i} \begin{bmatrix} \cos\phi_i\,(1-\cos(\kappa_i \ell_i)) \\ \sin\phi_i\,(1-\cos(\kappa_i \ell_i)) \\ \sin(\kappa_i \ell_i) \end{bmatrix}, \kappa_i \neq 0 \qquad (2)$$

and $R_i$is the corresponding rotation matrix obtained from the standard PCC construction. The full forward kinematics to the manipulator tip is the ordered product

$$T_{\text{tip}} = T_1(\kappa_1, \phi_1, \ell_1)\, T_2(\kappa_2, \phi_2, \ell_2) \cdots T_N(\kappa_N, \phi_N, \ell_N). \qquad (3)$$

For a tendon-driven section with $n_t$tendons routed at radius $r$and angular offsets $\alpha_t$, actuator lengths $\Delta_t$relate to $(\kappa_i, \phi_i)$through

$$\Delta_t = \kappa_i \ell_i\, r \cos(\phi_i - \alpha_t), t = 1, \dots, n_t, \qquad (4)$$

which provides the actuation Jacobian $J_{a,i} = \partial\Delta / \partial(\kappa_i, \phi_i)$used later in the optimisation gradient.

### 3.2 Cosserat-Rod Formulation with Auxiliary Stiffening Backbone

The PCC model neglects external load and shear, both of which are significant in medical contact tasks. We therefore adopt a Cosserat-rod description for load-aware optimisation. The manipulator backbone is parameterised by arclength $s \in [0, L]$, position $p(s) \in \mathbb{R}^3$, and orientation $R(s) \in SO(3)$, evolving according to

$$\dot{p}(s) = R(s)\, v(s), \dot{R}(s) = R(s)\, \hat{u}(s), \qquad (5)$$

where $v(s)$and $u(s)$are the linear and angular strain rates in the local frame, and $(\widehat{\;\cdot\;})$denotes the skew-symmetric map. Internal force $n(s)$and moment $m(s)$satisfy the static equilibrium equations

$$\dot{n}(s) = -\sum_{t=1}^{n_t} f_t\,(s) - f_e(s) - \rho\, g, \qquad (6)$$

$$\dot{m}(s) = -\dot{p}(s) \times n(s) - \sum_{t=1}^{n_t} l_t\,(s) - l_e(s), \qquad (7)$$

where $f_t, l_t$are tendon-induced force and moment, $f_e, l_e$are externally applied contact force and moment (e.g. tissue reaction), $\rho$is the linear mass density, and $g$is gravity. A linear constitutive law closes the system,

$$n(s) = R(s)\, K_{SE}(v(s) - v^*), m(s) = R(s)\, K_{BT}(u(s) - u^*), \qquad (8)$$

with $K_{SE} = \text{diag}(k_{SE}^x, k_{SE}^y, k_{SE}^z)$and $K_{BT} = \text{diag}(k_{BT}^x, k_{BT}^y, k_{BT}^z)$the shear/extension and bending/torsion stiffness matrices.


DOI: 10.46121/pspc.54.3.16

Power System Protection and Control
ISSN:1674-3415

For manipulators employing a slidable superelastic backbone of insertion depth $d \in [0, L]$(e.g. a Nitinol core sliding within a central lumen of a tendon-driven elastomeric body), the overlapped region $s \in [0, d]$exhibits combined stiffness

$$K_{BT}(s) = \begin{cases} K_{BT,\text{body}} + K_{BT,\text{backbone}}, & s \le d \\ K_{BT,\text{body}}, & s > d, \end{cases} \qquad (9)$$

so that $d$acts as a continuous stiffness-scheduling variable: $d = 0$recovers the fully compliant tendon-driven kinematics of Section 3.1, while $d \to L$approaches the stiffness of the auxiliary backbone material, at the cost of reduced achievable curvature for a given tendon actuation. Equations (5)–(9), together with boundary conditions enforcing force/moment continuity at $s = d$and prescribed tendon tension and external load at the tip, form a two-point boundary-value problem solved via a shooting method: an initial guess of $n(0), m(0)$is propagated forward using a fourth-order Runge–Kutta integrator, and the residual at the tip boundary condition is driven to zero using a nonlinear least-squares solver.

### 3.3 Manipulator Jacobian and Manipulability

Given either kinematic model, the tip-velocity Jacobian $J(q)$maps a generalised actuation-rate vector $\dot{q}$(tendon tensions, insertion depth rate) to tip twist,

$$\begin{bmatrix} \dot{p}_{\text{tip}} \\ \omega_{\text{tip}} \end{bmatrix} = J(q)\,\dot{q}, q = [\kappa_1, \phi_1, \dots, \kappa_N, \phi_N, d]^{\top}. \qquad (10)$$

The Yoshikawa manipulability index,

$$w(q) = \sqrt{\det(J(q)J(q)^{\top})}, \qquad (11)$$

quantifies the local capacity of the manipulator to generate tip motion in arbitrary directions and forms one component of the optimisation objective introduced below.

### 3.4 Compliance Ellipsoid

The task-space compliance matrix relates a small external force at the tip to the resulting tip displacement,

$$C(q) = \frac{\partial p_{\text{tip}}}{\partial f_{\text{tip}}} \in \mathbb{R}^{3\times 3}, \qquad (12)$$

computed numerically by finite-difference perturbation of $f_{\text{tip}}$within the Cosserat model. Eigen-decomposition $C = U\,\text{diag}(\lambda_1, \lambda_2, \lambda_3)\,U^{\top}$defines the *compliance ellipsoid*

$$\{\delta p : \delta p^{\top}(CC^{\top})^{-1}\delta p = 1\}, \qquad (13)$$

whose principal semi-axes $\lambda_1, \lambda_2, \lambda_3$indicate the directions and magnitudes of greatest tip deflection under unit force. In medical contact tasks the objective is typically to *minimise* the compliance-ellipsoid volume (or its dominant eigenvalue) in the direction of anticipated tissue contact, i.e. to make the manipulator locally stiff along the task-relevant axis while retaining compliance elsewhere for safety.

## MULTI-OBJECTIVE KINEMATIC OPTIMISATION FORMULATION

### 4.1 Decision Variables and Constraints

The optimisation seeks a generalised configuration $q^{\star} = [\kappa_1, \phi_1, \dots, \kappa_N, \phi_N, d]^{\top}$(or, for trajectory optimisation, a time sequence $q^{\star}(t)$) that best achieves a prescribed medical task subject to:

$$q_{\min} \le q \le q_{\max}\text{(actuator and insertion-depth limits)}, \qquad (14)$$

$$g_j(q) \le 0, j = 1, \dots, N_c\text{(anatomical collision-avoidance constraints)}, \qquad (15)$$

$$\parallel \tau \parallel_{\infty} \le \tau_{\max}\text{(tendon tension limit, to avoid tissue or material damage)}. \qquad (16)$$

Collision constraints $g_j(q)$are constructed as signed-distance functions between sampled points along the manipulator backbone $p(s; q)$and a segmented anatomical mesh (trocar wall, adjacent organ surfaces), obtained pre-operatively from CT/MRI data.

Power System Protection and Control
ISSN:1674-3415

### 4.2 Objective Terms

**(a) Target reaching error.** For a prescribed target pose $T_d = (R_d, p_d)$,

$$E_{\text{pos}}(q) = \| p_{\text{tip}}(q) - p_d \|_2^2, E_{\text{ori}}(q) = \| \log(R_d^\top R_{\text{tip}}(q))^\vee \|_2^2, \qquad (17)$$

where $\log(\cdot)^\vee$extracts the axis-angle vector from the relative rotation.

**(b) Dexterity / manipulability.** To avoid configurations near kinematic singularities, and to preserve local controllability for intra-operative micro-adjustment, we include

$$E_{\text{man}}(q) = -w(q), \qquad (18)$$

using the manipulability index of Eq. (11).

**(c) Task-space stiffness.** To ensure the manipulator can deliver a controlled force at the target (e.g. tissue palpation, fibre-optic contact for photodynamic therapy) without excessive tip deflection, we penalise the dominant compliance eigenvalue along the anticipated contact direction $\hat{n}_c$:

$$E_{\text{stiff}}(q) = \hat{n}_c^\top C(q)\, \hat{n}_c. \qquad (19)$$

**(d) Actuation effort.** To favour low tendon tension and conservative backbone insertion (reducing risk of material fatigue and excessive tissue contact force during approach),

$$E_{\text{eff}}(q) = \sum_{t=1}^{n_t} \tau_t^2 + \beta\, d^2, \qquad (20)$$

with $\beta$a weighting coefficient penalising unnecessary backbone insertion.

**(e) Obstacle clearance margin.** A smooth barrier term augments the hard constraints of Eq. (15) to encourage a safety margin $\delta_{\text{safe}}$:

$$E_{\text{obs}}(q) = \sum_j \max(0,\ \delta_{\text{safe}} - g_j(q))^2. \qquad (21)$$

### 4.3 Composite Objective

The multi-objective problem is scalarised via weighted summation,

$$q^\star = \arg\min_q\ [w_1 E_{\text{pos}}(q) + w_2 E_{\text{ori}}(q) + w_3 E_{\text{man}}(q) + w_4 E_{\text{stiff}}(q) + w_5 E_{\text{eff}}(q) + w_6 E_{\text{obs}}(q)] \text{s.t. (14)-(16)}, \qquad (22)$$

with weights $w_1, \dots, w_6 \geq 0$selected to reflect procedure-specific priorities (e.g. $w_1, w_2$dominant during approach, $w_4$dominant once the tip is in contact with tissue). Because the individual objectives are generally competing—maximal manipulability tends to favour low backbone insertion, whereas task-space stiffness favours deep insertion—the weighted-sum formulation is complemented by construction of the Pareto front via repeated solution of (22) over a grid of weight vectors, allowing the clinician or planning software to select an operating point rather than a single fixed trade-off a priori.

## NUMERICAL OPTIMISATION PROCEDURE

### 5.1 Two-Stage Solution Strategy

Direct joint optimisation of the full Cosserat-rod boundary-value problem (Eqs. 5–9) within an outer optimisation loop is computationally expensive, since each objective evaluation requires an inner shooting-method solve. We therefore adopt a two-stage strategy:

1. **Coarse search (PCC surrogate).** The PCC kinematics of Section 3.1 provide a closed-form, differentiable surrogate for $E_{\text{pos}}$, $E_{\text{ori}}$, and $E_{\text{man}}$. A gradient-based local optimiser (sequential quadratic programming, SQP) or, where the objective is expected to be strongly multi-modal due to obstacle constraints, a population-based evolutionary strategy (covariance matrix adaptation, CMA-ES) is used to obtain a candidate solution set $\{q^{(k)}\}$rapidly.
2. **Refinement (Cosserat model).** Each candidate is refined using the full Cosserat-rod model, including $E_{\text{stiff}}$and load-dependent shape correction, via a limited number of trust-region iterations. The Jacobian required for the trust-region step is obtained by central finite differences on $q$, exploiting the fact that the


**DOI:** 10.46121/pspc.54.3.16

Power System Protection and Control
ISSN:1674-3415

inner boundary-value solve is warm-started from the previous iterate, which substantially reduces shooting-method iteration count.

### 5.2 Gradient Approximation

For the PCC surrogate, the analytic Jacobian $\partial p_{\mathrm{tip}}/\partial q$follows directly from differentiating Eq. (3). For the Cosserat-refinement stage, the compliance matrix $C(q)$and the sensitivity $\partial p_{\mathrm{tip}}/\partial q$are approximated by central differences,

$$\frac{\partial p_{\mathrm{tip}}}{\partial q_i} \approx \frac{p_{\mathrm{tip}}(q+\epsilon_i e_i) - p_{\mathrm{tip}}(q-\epsilon_i e_i)}{2\epsilon_i}, \qquad (23)$$

with per-variable step size $\epsilon_i$scaled to the physical units of $q_i$(radians for curvature/plane angle, millimetres for insertion depth).

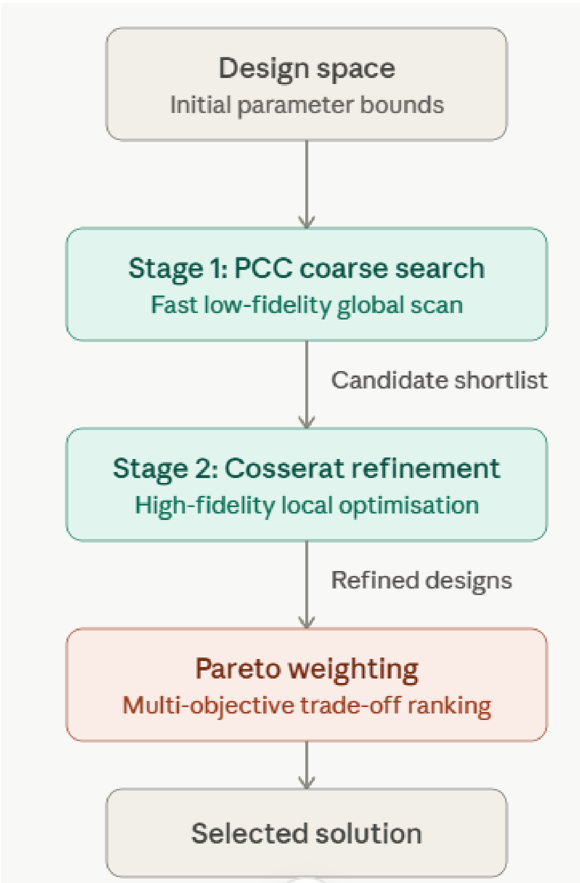


**Figure 1: a flowchart of the two-stage optimisation pipeline (PCC coarse search → Cosserat refinement → Pareto weighting).**

### 5.3 Constraint Handling

Box constraints (14) are enforced directly by the optimiser. Collision constraints (15) are implemented as inequality constraints in the SQP stage and as penalty terms during the CMA-ES stage, consistent with the corresponding solver's native constraint-handling mechanism. Tendon-tension limits (16) are checked post hoc at each candidate configuration using the Cosserat tendon-force model; infeasible candidates are discarded before refinement.

## CASE STUDY: LAPAROSCOPIC TARGETING OF A PANCREATIC LESION

To illustrate the framework, we consider a representative scenario motivated by soft-robotic laparoscopic photodynamic therapy: a two-segment tendon-driven manipulator with a central slidable superelastic backbone is inserted through a single laparoscopic port and must position its distal tip, carrying a diffusing optical fibre, against a simulated lesion on the anterior pancreatic surface while avoiding the stomach, transverse colon, and bile duct.

### 6.1 Task Specification

The manipulator has total length $L = 160$mm, outer diameter 20mm, and four tendons per segment routed at radius $r = 8$mm. The task specifies a target position $p_d$located approximately 110mm from the port along a curved approach path, with a desired tip-approach vector normal to the simulated lesion surface (orientation tolerance $\pm 5°$), and a minimum standoff clearance of 3mm from segmented organ boundaries elsewhere along the backbone. During therapeutic contact, the manipulator must maintain a tip compliance eigenvalue $\lambda_1$below a threshold representative of stable optical coupling, informed by the trend that backbone insertion substantially reduces tip compliance in the major axis of the compliance ellipsoid relative to the fully compliant (zero-insertion) configuration.

### 6.2 Objective Weighting

Two operating regimes are defined. During the *approach phase*, weights emphasise positional accuracy and obstacle clearance ($w_1 = w_2 = w_6 = 1, w_3 = 0.3, w_4 = 0, w_5 = 0.1$) with backbone insertion depth constrained near zero to preserve dexterity through the curved approach. During the *contact phase*, once the tip lies within a small neighbourhood of $p_d$, the weighting shifts to emphasise stiffness ($w_4 = 1$) and orientation accuracy ($w_2 = 1$), allowing $d$to increase toward the optimum determined by the trade-off described in Eq. (9).

### 6.3 Illustrative Outcome

Solving the two-stage optimisation of Section 5 for this scenario yields two qualitatively distinct behaviours consistent with the underlying mechanics. In the approach phase, the optimiser favours near-zero backbone insertion, exploiting the larger dexterous workspace of the fully compliant configuration to route the tip around the simulated colon boundary while satisfying the clearance constraint (21). As the tip enters the contact-phase neighbourhood, the optimal insertion depth increases toward an intermediate value rather than the maximum available depth—reflecting the same reachability/stiffness trade-off documented for backbone-stiffened soft manipulators, in which excessive insertion depth stiffens the structure to the point that tendon actuation can no longer achieve the required fine positional correction near the target, while insufficient insertion leaves the tip too compliant to maintain stable contact under the reaction force of tissue engagement. This non-monotonic optimum is a direct manifestation of objective terms $E_{\text{stiff}}$and $E_{\text{man}}$acting in opposition in Eq. (22), and would not be discoverable using a stiffness-agnostic PCC-only planner that treats $d$as fixed rather than as an optimisation variable.

### 6.4 Sensitivity to Weighting

Repeating the contact-phase optimisation over a grid of $(w_3, w_4)$traces a Pareto front between manipulability and tip stiffness. Configurations near the manipulability-favouring end of the front retain a larger set of feasible tendon actuations for fine tip-orientation correction but exhibit a larger major-axis compliance eigenvalue, increasing the risk of tip drift during fibre-tissue contact; configurations near the stiffness-favouring end reduce compliance substantially at the cost of a narrower actuation range for last-moment orientation correction. This front provides a principled basis for pre-operative selection of an operating point appropriate to the specific therapeutic requirement (e.g. photodynamic dose delivery, which tolerates modest positional drift, versus needle-guided biopsy, which does not).

## DISCUSSION

### 7.1 Implications for Medical Manipulator Design

The case study illustrates a general principle relevant to the design, not merely the control, of hybrid-stiffness soft manipulators for medical intervention: because the optimal stiffness-modulation depth is task- and phase-dependent, manipulator designs that expose insertion depth (or an equivalent stiffness variable) as a continuously controllable parameter—rather than a binary "soft" or "locked" state—offer a materially larger feasible region in the combined workspace–stiffness objective space. This supports design choices favouring electromechanically actuated, continuously variable stiffness mechanisms over shape-memory or jamming-based approaches whose response time or discretisation may be too coarse to track the approach-to-contact transition modelled in Section 6.

### 7.2 Computational Considerations

The two-stage optimisation strategy of Section 5 renders the Cosserat-rod refinement tractable for pre-operative planning, where solve times on the order of a second per configuration (as reported for comparable Cosserat-rod shooting-method implementations) are acceptable. Intra-operative re-optimisation in response to organ motion or tissue deformation, however, requires either a substantially faster inner solver—for example, a precomputed Jacobian via the sensitivity equations of the boundary-value problem rather than finite-difference approximation—or a reduced-order, PCC-based fallback with periodic Cosserat correction. This remains an open engineering trade-off between model fidelity and control-loop bandwidth.

### 7.3 Limitations

The present formulation makes several simplifying assumptions consistent with the underlying continuum-mechanics literature: friction between tendons, the auxiliary backbone, and the elastomeric body is neglected; the backbone and manipulator medial axis are assumed concentric; and external loads are modelled as point forces/moments at the tip or along discretised contact locations rather than as distributed, deformable-tissue contact. Extending the optimisation objective to incorporate a validated tissue-contact model—rather than treating $f_e$ as a prescribed input—would allow the framework to jointly optimise approach trajectory and applied force profile, which is particularly relevant for tasks involving tissue retraction or palpation rather than static fibre-optic contact. Additionally, the weighted-sum scalarisation of Eq. (22) requires a priori weight selection or repeated Pareto-front sampling; a natural extension is to solve the true multi-objective problem using Pareto-based evolutionary algorithms (e.g. NSGA-II) to generate the trade-off surface in a single optimisation run, at increased computational cost.

### 7.4 Toward Closed-Loop Kinematic Optimisation

Finally, the framework as presented is a planning-time (open-loop) optimisation. Coupling it with intra-operative shape sensing—for example, fibre Bragg grating or electromagnetic tracking of the manipulator backbone—would allow the compliance matrix $C(q)$ and manipulability index $w(q)$ to be updated online against measured, rather than modelled, shape, closing the loop between the kinematic optimiser and the physical manipulator state and compensating for the model-order-reduction errors inherent in both the PCC and Cosserat formulations.

## CONCLUSION

This paper presented a kinematic optimisation framework for soft robotic manipulators intended for medical intervention, unifying piecewise constant-curvature and Cosserat-rod kinematic models within a multi-objective optimisation formulation that jointly considers target-reaching accuracy, manipulability, task-space compliance, actuation effort, and anatomical obstacle clearance. A key contribution is the explicit treatment of auxiliary stiffness-modulation depth as a first-class decision variable, motivated by hybrid-stiffness continuum manipulator designs that combine a compliant elastomeric body with a slidable superelastic backbone. A two-stage optimisation procedure—coarse PCC-based search followed by Cosserat-model refinement—was proposed to render the formulation computationally tractable for pre-operative planning. A representative laparoscopic targeting case study demonstrated that joint optimisation of kinematic configuration and stiffness-modulation depth yields a non-trivial, phase-dependent optimum that balances dexterous reachability during approach against positional stability during tissue contact, a trade-off inaccessible to stiffness-agnostic planners. Future work will address intra-operative closed-loop re-optimisation under tissue deformation, incorporation of distributed contact-mechanics models, and Pareto-based multi-objective solvers to replace the weighted-sum scalarisation adopted here.

## REFERENCES

1. **Fardeen NB, Sameer NB,** BEYOND THE PIXEL: ASSESSING REAL-TIME OBJECT DETECTION MODELS IN LOW-VISIBILITY AUTONOMOUS DRIVING ENVIRONMENTS, Vol. 53 No. 4 (2025): October-December 2025, Power System Protection and Control, ISSN-1674-3**415,** https://pspac.info/index.php/dlbh/article/view/371
2. **Fardeen NB, Sameer NB,** AUTOMATIC CLASSIFICATION OF LEUKEMIA CELLS VIA FLOW CYTOMETRY AND MITRAL REGURGITATION DETECTION USING MACHINE LEARNING

ALGORITHMS, Vol. 49 No. 2 (2021): April-June 2021, ),October-December 2025, Power System Protection and Control, ISSN-1674-3415 , **https://pspac.info/index.php/dlbh/article/view/361**

3. **Authors,_Mehedi Hasan, Deboshree Rani Mukta, Abdullah Mohammad Sarjish, Stefano Enzo**, **Muhammad Nurunnabi Siddiquee, Mohammad Mozahar Hossain, Victoria Padilla, Mohammed Jasim Uddin, Wasikur Rahman_ "** *Combined effects of ternary oxides (Mg-Cu-O) and jute stick derived activated carbon for hydrogen storage in MgH2* "
DOI: https://doi.org/10.1007/s11356-025-36394-4 , **Apr-2025**
4. **Authors: _Md. Wasikur Rahman Md. Sabbir Ahmed, Selim Reja, Sk Md Ali Zaker Shawon, Farhana Nazmin, Abdullah Mohammad Sarjish, Yousuf Ali, M. Azizur R. Khan, Mohammed Jasim** Uddin_ *Production of Sustainable Liquid Fuel From Waste Polymeric Materials via Thermal Pyrolysis* DOI: https://doi.org/10.1155/er/1449087 ,
5. **Sarjish, Abdullah Mohammad, et al.** " *Nano Polymers for Clean Energy Solutions* ." Nanostructured Polymers: Synthesis and Performance. Singapore: Springer Nature Singapore, 2026. 461-495. https://doi.org/10.1007/978-981-95-3581-1_18 , **Feb-2026**
6. **Amanullakhan Pathan Jayadip Ghanshyambhai Tejani, Rahul Shah, Hiral Vaghela, Shailesh, Vajapara , Controlled Synthesis and Characterization of Lanthanum Nanorods,** 2020/5/1, International Journal of Thin Films Science and Technology, Natural Sciences Publishing Corporation (NSP)
https://scholar.google.com/citations?view_op=view_citation&hl=en&user=efbNMkwAAAAJ&citation_for_view=efbNMkwAAAAJ:M3NEmzRMIkIC
7. **Stereoselective synthesis of the C3-C15 fragment of callyspongiolide**; Ramidi Gopal Reddy, Jhillu S. Yadav and Debendra K. Mohapatra. (Tetrahedron Letters. 2018, 59, 3579-3582). https://doi.org/10.1016/j.tetlet.2018.08.041,
https://www.sciencedirect.com/science/article/pii/S0040403918310426
8. **Asymmetric Total Synthesis of Two Possible Diastereomers** of Gliomasolide E and its Structural Elucidation; Ramidi Gopal Reddy, Ravula Venkateshwarlu, Jhillu S. Yadav and Debendra K. Mohapatra. (J. Org. Chem. 2017, 82(2), 1053-1063). https://doi.org/10.1021/acs.joc.6b02611, , https://pubs.acs.org/doi/abs/10.1021/acs.joc.6b02611
9. **Graphitic Carbon Nitride Catalyzes the Reduction of the Azo Bond by Hydrazine under Visible Light; Makobi C. Okolie**, Glory G. Ollordaa, Gopal R. Ramidi, Xin Yan, Yufeng Quan, Qingsheng Wang and Yingchun Li. (Nanomaterials 2024, 14(17), 1402), https://doi.org/10.3390/nano14171402, https://www.mdpi.com/2079-4991/14/17/1402
10. **Lakshmi Rahul Reddy Mareddy, 2026, IJCNIS,**
https://www.ijcnis.org/index.php/ijcnis/article/view/8735
11. **Lakshmi Rahul Reddy Mareddy, 2026, ICAA,**
**,https://eudoxuspress.com/index.php/pub/article/view/4780/3569**
12. **Lakshmi Rahul Reddy Mareddy, 2026, IJCMI ,**
**https://www.ijcmi.in/index.php/ijcmi/article/view/70**
13. **Rangavinay Teja Royal Jagga** , 2026, https://ieeexplore.ieee.org/document/11448495
14. **Rangavinay Teja Royal Jagga , 2026, https://ieeexplore.ieee.org/document/11448514**
15. **Rangavinay Teja Royal Jagga , 2026, https://ieeexplore.ieee.org/document/11448337**
16. **Rangavinay Teja Royal Jagga , 2026, https://ieeexplore.ieee.org/document/11497560**

17. **Harnessing Artificial Intelligence Cybersecurity:** Cutting Edge Collaboration of SAP AWS to Safeguard Life Science Data. 2026 https://doi.org/10.1109/aiei69164.2026.11497833
18. **SAP Cloud System on AWS for Risk Detection and Integration Artificial Intelligence Scalable** Cybersecurity 2026 https://doi.org/10.1109/aiei69164.2026.11497435
19. **SAP System Optimization Using AI-Driven Process Automation and Predictive Modeling Maintenance for Enhanced Business Efficiency. 2025** https://doi.org/10.1109/computingcon64838.2025.11376613
20. https://ieeexplore.ieee.org/abstract/document/11376613
21. https://ieeexplore.ieee.org/abstract/document/11497833
22. https://ieeexplore.ieee.org/abstract/document/11497435
23. **Kaleshwar Aryasomayajula**, PREVENTING BIAS IN AI-BASED DECISION-MAKING: ANALYZING TECHNIQUES TO REMOVE UNFAIR PREJUDICE IN ALGORITHMIC OUTCOMES, Vol. 50 No. 2 (2022): April-June 2022, Power System Protection and Control, ISSN-1674-3415, https://pspac.info/index.php/dlbh/article/view/294
24. **Kaleshwar Aryasomayajula, MODERN** DEVELOPMENT PRACTICES: INVESTIGATIONS INTO SERVERLESS COMPUTING, LOW-CODE/NO-CODE PLATFORMS, AND DEVELOPER PRODUCTIVITY IN REMOTE ENVIRONMENTS, Vol. 50 No. 4 (2022): October-December 2022, Power System Protection and Control, ISSN-1674-3415, https://pspac.info/index.php/dlbh/article/view/364
25. **Kaleshwar Aryasomayajula**, Micro services: “A Comparative Analysis of Monolithic vs. Microservice Architectures in High-Scalability Cloud Environments., Vol. 51 No. 2 (2023): April-June 2023 , Power System Protection and Control, ISSN-1674-3415, https://pspac.info/index.php/dlbh/article/view/374
26. **Alam, M. Z., Rahman, R., Sozib, H. M., Ahmed**, H., Hossain, A., Sabeena, A. A., Tasnim, A. F., Ahmed, F., Sarkar, M. I., & Erdei, T. I. (2026). Enhancing Thyroid Disease Diagnosis with Machine Learning and Counterfactual Explainable AI. IEEE Access, 1–1. https://doi.org/10.1109/access.2026.3663497
27. **Yeasmin, S., Semi, M. M. A., Rony, M. K. K., Das, S., Sabeena, A. A., Rahman, R., Biswas, B., Ahmed, F., & Hossain, A. (2025).** Artificial Intelligence for Mental Health Monitoring: A Solution for Digital Behavioral Health Care and Education—An Umbrella Review. Health Science Reports, 9(1), e71703. https://doi.org/10.1002/hsr2.71703
28. **Hasan, S., Rahman, K. A., Ahmed, F., & Hossain, A. (2026). An integrated AI-driven framework for** maternal resource intelligence shortages across U.S. hospitals. Integrative Biomedical Research, 10(1), 1–8. https://doi.org/10.25163/biomedical.10110694
29. **29: Riipa, M. B., Ahmed, F., Rony, M. K. K., Hossain, A., Islam, A., Utsho, M. R., Kamal, M. B., Sharmin, S., &** Tasnim, A. F. (2026). The role of artificial intelligence in predicting cardiovascular outcomes: a systematic review and meta-analysis. Biostatistics & Epidemiology, 10(1). https://doi.org/10.1080/24709360.2026.2670804
30. **30: Semi, M. M. A., Das, S., Utsho, M. R., Hossain,** A., Kamal, M. B., Sizan, A. A., Tasnim, A. F., Yeasmin, S., & Parvin, M. R. (2026). Artificial Intelligence in Public Health Education: A Scoping Review of workforce competency development. Health Science Reports, 9(3). https://doi.org/10.1002/hsr2.72066

31. **Ahmed, F., Hasan, S., Hossain, A., & Rahman, K. A. (2026). Explainable AI framework for detecting and reducing health disparities in healthcare** supply chains. Journal of AI, ML and DL, 2(1), 1–8. https://doi.org/10.25163/ai.2110685
32. **Godavari Modalavalasa," SCALABLE CLOUD SOLUTIONS THROUGH ARTIFICIAL INTELLIGENCE GOVERNANCE**: APPLICATIONS IN HEALTHCARE AND FINANCIAL SYSTEMS", Vol. 54 No. 1 (2026): January-March 2026, Power System Protection and Control, ISSN-1674-3415, https://pspac.info/index.php/dlbh/article/view/219, , DOI: https://doi.org/10.46121/pspc.54.1.25
33. **Godavari Modalavala**sa, AUTONOMOUS DATA ENGINEERING PIPELINES: A POLICY-DRIVEN ARCHITECTURE FOR SECURE AND SCALABLE CLOUD-NATIVE ANALYTICS, Vol. 53 No. 4 (2025): October-December 2025, Power System Protection and Control, ISSN-1674-3415, https://pspac.info/index.php/dlbh/article/view/181, DOI: https://doi.org/10.46121/pspc.53.4.25
34. **Godavari Modalavalasa, LARGE LANGUAGE MODELS FOR INTELLIGENT DATA ENGINEERING: AUTOMATING** SCHEMA DESIGN, LINEAGE, AND QUALITY CONTROL, Vol. 50 No. 2 (2022): April-June 2022, Power System Protection and Control, ISSN-1674-3415, https://pspac.info/index.php/dlbh/article/view/183 , DOI: https://doi.org/10.46121/pspc.50.2.4
35. **Godavari Modalavalasa**, FEDERATED LEARNING FOR ENTERPRISE CLOUD DATA ENGINEERING: ARCHITECTURE, SECURITY, AND GOVERNANCE CHALLENGES, Vol. 51 No. 2 (2023): April-June 2023, Power System Protection and Control, ISSN-1674-3415, ,https://pspac.info/index.php/dlbh/article/view/184, DOI: https://doi.org/10.46121/pspc.51.2.5
36. **Godavari Modalavalasa, AI**-DRIVEN DATA GOVERNANCE: INTELLIGENT METADATA, LINEAGE, AND COMPLIANCE AUTOMATION IN CLOUD DATA PLATFORMS, Archives / Vol. 52 No. 1 (2024): January-March 2024 /, Power System Protection and Control, ISSN-1674-3415, https://pspac.info/index.php/dlbh/article/view/182, DOI: https://doi.org/10.46121/pspc.52.1.3
37. **Hima Bindu Lekkala, VishnuVardhan Bandar**i , AUTONOMOUS WORKFLOW OPTIMIZATION USING MULTI AGENT AI SYSTEMS AI AGENTS MANAGE STATIONS, WIP, AND TASK HANDOFFS, Vol. 54 No. 2 (202): April-June 2026, Power System Protection and Control, ISSN-1674-3415, https://pspac.info/index.php/dlbh/article/view/306 , DOI: https://doi.org/10.46121/pspc.54.2.08
38. **Lekkala, H. B., & Bandari, V. V. (2026). Autonomous workflow optimization using multi-agent AI systems:** AI agents manage stations, WIP, and task handoffs. *Power System Protection and Control*, 54(2), 95–101. http://pspac.info/index.php/dlbh/article/view/306
39. **Bandari, V. V., & Lekkala, H. B. (2024). Physics-informed reinforcement learning for real-time control of complex manufacturing processes**. *Power System Protection and Control*, 52(2), 164–170. https://pspac.info/index.php/dlbh/article/view/343
40. **Lekkala, H. B., & Bandari, V. V. (2025). AI-based energy-aware scheduling and process optimization** in engineer-to-order smart manufacturing systems. *Power System Protection and Control*, 53(1), 30–36. http://pspac.info/index.php/dlbh/article/view/341
41. **Bandari, V. V., & Lekkala, H. B. (2026). AI-driven digital** thread framework for end-to-end lifecycle optimization in ETO manufacturing systems. *Power System Protection and Control*, 54(2), 318–325. http://pspac.info/index.php/dlbh/article/view/340
42. **Lekkala, H. B., & Bandari, V. V. (2026). Deep learning** for weld defect detection using CNN or vision transformers fusion detection. *Power System Protection and Control*, 54(2), 151–158. https://pspac.info/index.php/dlbh/article/view/314

43. **Bandari, V. V., & Lekkala, H. B. (2024). AI-based operator** behavior monitoring and cost optimization using digital traceability in manufacturing systems. *Power System Protection and Control*, 52(1), 38–45. https://pspac.info/index.php/dlbh/article/view/342

44. **Shreyas Jayaprakash,** MACHINE LEARNING-DRIVEN VERIFICATION: USING ML TO OPTIMIZE COVERAGE ANALYSIS, PREDICT SIMULATION RUNTIMES, AND AUTO-GENERATE TESTBENCHES, Vol. 54 No. 2 (2026): April-June 2026, Power System Protection and Control, ISSN-1674-3415, https://pspac.info/index.php/dlbh/article/view/391

45. **Mohammed Shafi Kundiladi,** EVENT-DRIVEN IMAGE AND VEHICLE STATUS MANAGEMENT FOR LOW-POWER IOT DIGITAL LICENSE PLATES, Vol. 53 No. 3 (2025): July-September 2025, Power System Protection and Control, ISSN-1674-3415, https://pspac.info/index.php/dlbh/article/view/175 DOI: https://doi.org/10.46121/pspc.53.3.17

46. Controlled Synthesis and Characterization of Lanthanum Nanorods, **Author(s), Jayadeep Tejani, Rahul Shah, Hiral Vaghela, Shailesh Vajapara, Amanullakhan Pathan**, doi:10.18576/ijtfst/090205, URL: https://www.naturalspublishing.com/Article.asp?ArtcID=20705, May-2020

47. **Kunal Kapoor**, **Apr 2026,** Relation Extraction and NER through Fine Tuned BERT model with transfer Learning, https://ieeexplore.ieee.org/document/11472214/metrics#metrics

48. **Harender Bisht**, Human–AI Collaboration in Insurance Fraud Detection: Ethical Cloud-Native Architectures for Fair and Transparent Decision Support, **Volume 2026, Issue 1,** https://doi.org/10.52710/cfs.873

49. **Harender Bisht,** Ethical AI-Augmented Compliance Systems: Architectural Innovations for Cloud-Native Financial and Insurance Data Integrity, **Vol. 11 No. 1s (2026) ,** https://doi.org/10.52783/jisem.v11i1s.14056

50. **Harender Bisht**, Governance-By-Design For AI-Based Insurance Fraud Detection: Auditability, Accountability, And Regulatory Traceability, **Archives / Vol. 9 No. 1 (2026)** ,https://doi.org/10.63278/jicrcr.vi.3620

51. **Harender Bisht,** Operationalizing Explainable AI in Insurance Fraud Detection: From Model Transparency to Decision Justification, **Vol. 35 No. 1 (2026): JOCAAA**,

52. **A. MahendraVardhan and S. Sridhar,** "Determining False Positive Analysis of Software Vulnerabilities with Predefined Scan Rules using Random Forest Classifier and Decision Tree Technique," **2022 4th International Conference on Advances in Computing**, Communication Control and Networking (ICAC3N), Greater Noida, India, 2022, pp. 622-625, **DOI: https://doi.org/10.1109/ICAC3N56670.2022.10074458**

53. **Amilineni, M.V. 2025**. Audit-Safe Agentic RAG Framework for Regulated Enterprise Systems: A Trustworthy AI Architecture for SAP, Finance, Healthcare, and Government Workflows. INTERNATIONAL JOURNAL OF ADVANCES IN SIGNAL AND IMAGE SCIENCES. (Jan. 2025), 34– **DOI: https://doi.org/10.29284/7fjzk883**

54. **Islam, Imtiaz (Annotator), Goard, Michael (Annotator), Daves, Daniel (Annotator),** Credit Card Fraud Detection: A Comparative Study of Anomaly Detection and Supervised Learning under Extreme Class Imbalance, Published **May 5, 2026** | Version v1, **DOI: 10.5281/zenodo.20032207**

55. **Deepa Nagalavi; Shankar Balla Microsoft, USA; Pushpalatha. M; Nashwan Adnan Othman; Malik Bader Alazzam; A. Balakumar,** Enhancing Real-Time Language Processing via Advanced PET Signal Analysis and Deep Learning, ***06-07 June 2025***, DOI: 10.1109/ICICKE65317.2025.11136561 , https://ieeexplore.ieee.org/document/11136561
56. **Venkata Sai Aditya Kondru,FMR, Carmel, USA ,; Shankar Balla; Dhavalkumar Thakar; Dheeraj Velaga; Sri Lekha Bandla,** Intelligent Human–Computer Interaction for Navigation Control Through Vision-Based Hand Gesture Recognition, Conferences >2026 IEEE 15th International , **Date of Conference:** ***07-09 April 2026***,**Date Added to IEEE** ***Xplore***: 08 May 2026 **DOI:** 10.1109/CSNT69054.2026.11502317 , https://ieeexplore.ieee.org/abstract/document/11502317
57. **SUDIPKUMAR GHANVAT , AISHWARYA BADLANI, SHREYA SANDEEP JOSHI,** MARKETING EFFECTIVENESS IN THE POST-COOKIE ERA: A COMPARATIVE ANALYSIS OF FIRST PARTY AND ZERO-PARTY DATA STRATEGIES ON CAMPAIGN PERFORMANCE AND CUSTOMER EQUITY, **VOL. 31 NO. 4 (2023):** JOCAAA , HTTPS://WWW.EUDOXUSPRESS.COM/INDEX.PHP/PUB/ARTICLE/VIEW/3940
58. **Navin Chhibber,; Deepak Singh; Anokh Kishore, Capital One, USA; Nikita Chawla; K. Anguraj,** Multi-Granular Attention-Driven Reinforcement Learning Framework for Web Intelligent Enhancement Systems, , **11 June 2026**, https://ieeexplore.ieee.org/document/11483386
59. **Kapoor K, et al. AI-Driven COVID-19 Care**: Analytics, Scheduling & Geo-Access. International Journal of Drug Delivery Technology (IJDDT). **2026;16(65S):Article** 136. Available at: https://impactfactor.org/PDF/IJDDT/16/IJDDT,Vol16,Issue65s,Article136.pdf
60. **Kilama, D. (2026). Mechanisms of Chinese** Aid to Africa: A Comparative Analysis with Western Philanthropic and Development Models. Interdisciplinary Social Research, 2(1).DOI: https://doi.org/10.64220/isr.v2i1.011,
61. https://scholarlysummit.com/journals/isr/articles/mechanisms-of-chinese-aid-to-africa-a-comparative-analysis
62. **Kilama, D. (2026). Beyond Altruism**: Analyzing China's Strategic Motivations Behind Development Aid to Africa. *Interdisciplinary Social Research, Volume 2 (2026)*(Issue 1), DOI: . https://doi.org/10.64220/isr.v2i1.012, Beyond Altruism: Analyzing China's Strategic Motivations Behind Development Aid to Africa
63. Anumolu DPK, Veena B, Afreen SS, Bandla J, Lakshmi KC, Pulusu VS. In vitro models for studying drug metabolites and metabolizing enzymes: A comprehensive review. Int J Pharm Investig. 2026;16(3):885–91. Available from: http://dx.doi.org/10.5530/ijpi.20260116
64. Asgar Z, Kumar G, Khandelwal P, Pratap B, Gurjar V, Baluni A, et al. Utility of contrast-enhanced computed tomography abdomen in Intestinal Obstruction. Int J Drug Deliv Technol. 2026;16(32s). Available from: http://dx.doi.org/10.25258/ijddt.16.32s.4
65. Anumolu DP, Ramatulasi J, Ashok G, Afreen SS, Mathew C, Shakar PV. Synthesis and characterization of MIP ghost approach for selective extraction of empagliflozin and quantification by liquid chromatography. J Chromatogr Sci. 2025;63(2). Available from: http://dx.doi.org/10.1093/chromsci/bmaf008.
66. Anumolu DPK, Naraparaju S, Addada SB, Pagidipally V, Pulusu VS, Afreen SS. Synthesis of silver nanoparticles using Ecbolium ligustrinum leaves: Characterization through advanced analytical techniques. Nanotechnol Percept . 2024;710–8. Available from: http://dx.doi.org/10.62441/nano-ntp.vi.3618

67. Naraparaju S, Mukti A, Anumolu DP, Chaganti S. Development and validation of a spectrofluorimetric method for the quantification of capecitabine in bulk and tablets. Turk J Pharm Sci [Internet]. 2023;20(4):234–9. Available from: http://dx.doi.org/10.4274/tjps.galenos.2022.46364
68. Naraparaju S, Yamjala P, Chaganti S, Anumolu DP. Spectrophotometric quantification of atomoxetine hydrochloride based on nucleophilic substitution reaction with 1,2-naphthoquinone-4-sulfonic acid sodium salt (NQS). Turk J Pharm Sci [Internet]. 2024;20(6):405–11. Available from: http://dx.doi.org/10.4274/tjps.galenos.2022.09147.
69. Anumolu PD, Shakar PV, Tulasi JR, Soujanya C, Afreen SS, Ashok G. Concurrent discriminative emission intensity quantification of Fexofenadine hydrochloride and Montelukast Sodium. Orient J Chem [Internet]. 2022;38(6):1364–8. Available from: http://dx.doi.org/10.13005/ojc/380605
70. Anumolu PD, Gurrala S, Menkana S, Mathew C, Srimantula L. Application of fluorotag in quantification of metformin in tablet dosage form and biological samples. The Thai Journal of Pharmaceutical Sciences [Internet]. 2022;46(1):93–8. Available from: http://dx.doi.org/10.56808/3027-7922.2550
**71.** Gurrala S, Raj S, Cvs S, Anumolu PD. Quality-by-design approach for chromatographic analysis of metformin, empagliflozin and linagliptin. J Chromatogr Sci [Internet]. 2022;60(1):68–80. Available from: http://dx.doi.org/10.1093/chromsci/bmab030
**72.** Gurrala S, Raj S, Cvs S, Anumolu DP, Naraparaju S, Nizampet H. Response surface methodology in spectrophotometric estimation of saxagliptin, derivatization with MBTH and ninhydrin. Turk J Pharm Sci [Internet]. 2022;19(1):9–18. Available from: http://dx.doi.org/10.4274/tjps.galenos.2021.93195
73. ebster, R. J., & Jones, B. A. (2010). Design and kinematic modeling of constant curvature continuum robots: A review. *The International Journal of Robotics Research*, 29(13), 1661–1683.
74. Rucker, D. C., & Webster, R. J. (2011). Statics and dynamics of continuum robots with general tendon routing and external loading. *IEEE Transactions on Robotics*, 27(6), 1033–1044.
75. Dupont, P. E., Lock, J., Itkowitz, B., & Butler, E. (2010). Design and control of concentric-tube robots. *IEEE Transactions on Robotics*, 26(2), 209–225.
76. Trivedi, D., Rahn, C. D., Kier, W. M., & Walker, I. D. (2008). Soft robotics: Biological inspiration, state of the art, and future research. *Applied Bionics and Biomechanics*, 5(3), 99–117.
77. Burgner-Kahrs, J., Rucker, D. C., & Choset, H. (2015). Continuum robots for medical applications: A survey. *IEEE Transactions on Robotics*, 31(6), 1261–1280.
78. Gravagne, I. A., & Walker, I. D. (2002). Manipulability, force, and compliance analysis for planar continuum manipulators. *IEEE Transactions on Robotics and Automation*, 18(3), 263–273.
79. Manti, M., Cacucciolo, V., & Cianchetti, M. (2016). Stiffening in soft robotics: A review of the state of the art. *IEEE Robotics & Automation Magazine*, 23(3), 93–106.
80. Yang, Y., Li, Y., & Chen, Y. (2018). Principles and methods for stiffness modulation in soft robot design and development. *Bio-Design and Manufacturing*, 1(1), 14–25.